Study of an Origami Crashbox Through Metamodels,
José Eduardo C. S. Silva, Larissa Driemeier and Marcílio Alves, ABCM, Sao Carlos, SP, Brazil, April 15th to 17th, 2019

STUDY OF AN ORIGAMI CRASHBOX THROUGH METAMODELS

José Eduardo Corrêa Santana Silva [1]; Larissa Driemeier [1] and Marcílio Alves [1]

[1] Group of Solid Mechanics and Structural Impact, University of São Paulo. Av. Prof. Mello Moraes, 2231 – São Paulo, SP, 05508-030

Abstract: An Energy Absorption Device is a structure created with the main objective of absorbing impact load energy. Such a device, in the form of an origami crash box is here studied using Design of Experiment, DOE, and Metamodeling techniques. The main idea is to use the results of a DOE run to create an approximation of the response variables over the design space. An optimization is performed on the Metamodel, allowing one to elect a set of parameters which will give the best performance of the objective function. The output responses are used to calculate the energy absorbed and the initial peak force and these objective functions guide the optimization procedure. In this paper, a Polygon-sided origami crashbox is optimized considering the number of polygonal sides, wall thickness, quantity of modules, side length and crest length. The so optimized origami crashbox is shown to perform better than one steamed from the automotive industry, being four times lighter.

Keywords: Crash Box, Origami, Energy Absorbers, Metamodels, Optimization, FEM, DOE.

INTRODUCTION

Known as crashworthiness capacity, a vehicle is currently designed specially to protect its occupant integrity in an eventual impact (Witteman, 1999; Bois et al., 2004; Ghannam et al., 2011; Lee et al., 2013). The energy absorption by the vehicle structure is the main concern in passive safety. In this way, most of the improvement can be attributed to the use of subcomponents able to buckle in a controlled and progressive way (Hsu; Jones, 2004; Kokkula et al., 2006; Karagiozova; Alves, 2008).

The concept and development of impact attenuation systems through controlled kinetic energy dissipation has drawn much attention from scientists and engineers in the past recent years, particularly in the context of car safety. According to Lu and Yu (2003), energy absorbers should keep the reactive force below a threshold which will cause injury, distributing the load, for example, over a long stroke. Moreover, irreversible impact energy conversion, stable and repeatable deformation modes, maximum specific energy absorption capacity and low cost are important characteristics for an impact energy absorber. In Alghamdi (2001), ways to dissipate plastic energy through several deformation modes are described, including axial compression. Axial compression in tubes has a relatively long deformation course, high specific energy absorption, SEA, and mechanical simplicity, being widely applied in industry. The main energy dissipation mechanism for this kind of device is the material plastic deformation (Ma, 2011).

Figure 1 illustrates a practical energy absorber load-deflection response. The peak force (F_{max}) is the highest value reached by the reaction force during the crushing process, and the average force (F_{mean}) is the total absorbed energy divided by the crushing length (δ_{crush}). Accordingly, in energy absorption applications a typical design requirement is related to the SEA, defined as the energy absorbed per unit mass of crashed material. The relation between average and peak force is called Load Uniformity (LU, as defined in Ma (2011)). In general, an improvement in SEA is obtained reducing the tube thickness or increasing the tube length or aspect ratio.

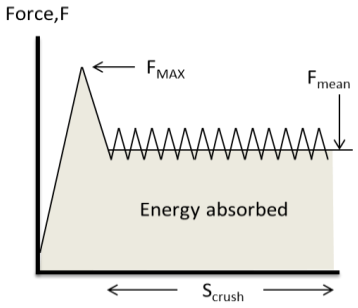

Figure 1 - Practical energy absorber load-deflection response.

Particularly, multi-corner tubes have several failure modes, depending on the aspect ratio, that is, width *(b)/* thickness *(t)* relation. Very thin tubes, $b/t \sim 100$, usually fail in non-compact modes, as shown in Fig. 2. This is an undesired deformation mode, from energy absorption point of view, because it could result in a global Euler buckling, reducing drastically the performance of the device. Tubes with moderate thickness usually buckle in symmetrical mode, as shown in Fig. 2, right side.

(a) (b)

Figure 2 – Non-compact buckling mode (a) and symmetrical (b).

Pioneer works from (Thorton; Mahmood; Magee, 1983), (Reid; Reddy; Gray, 1986), (Abramowicz; Wierzbicki, 1988), and later, (Tarlochan; Ramesh, 2012), (Lanzerath; Schilling, 2003), (Vignesh; Rao; Bade, 2018), among others, studied the progressive buckling of foam filled columns and the efficiency of the system in the absorption of energy. Shinde and Mali (2018) presented a comparison on energy absorption performance between metallic and non-metallic material, in vehicle safety.

Prefabricated polymeric reinforcements inside tubes are a good option to increase stiffness in regions where large deformations are expected (Matsumoto; Driemeier; Alves, 2012). These reinforcements have good performance in collision tests and a low weight. Also, different tube geometries are proposed in the literature. Many authors compared crashworthiness of thin-walled tubes, with different cross sections or load directions (Asanjarani; Mahdian; Dibajian, 2018; Sadjad; Mohammad-Hossein; Sobhan, 2018). Comi and Driemeier (2018), proposed tubes filled with resonant metamaterials. Isaac and Oluwole (2016) studied the energy absorption improvement of circular tubes when externally press-fitted ring is added to the tube.

The use of origami like crashboxes was first explored by Ma (2011) and later by Ma and You (2013), Zhou et al. (2016) and Ma, Song and Chen (2018). It consists of a thin-walled tube with sides shaped as origami patterns. In order to reduce the peak load Ma (2011) introduced geometric imperfections on the tube surface. The proposed origami crashbox induce folding patterns well fitted kinetic energy absorption. Also, most of origami shapes are developable: origami patterns can be manufactured on tube surfaces, with small distortions.

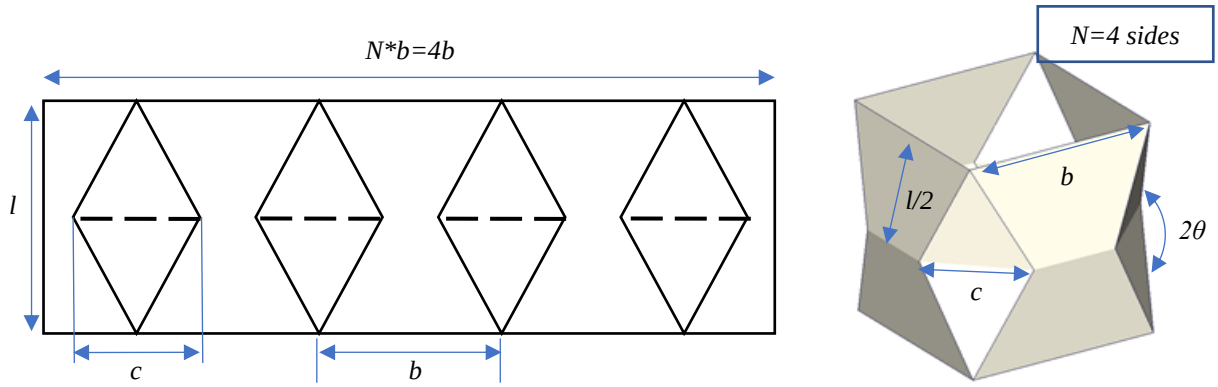

Figure 3 – Origami pattern for square tubes. On the left, the module unfolded. On the right, the folded module. Figure based on (Ma, 2011)

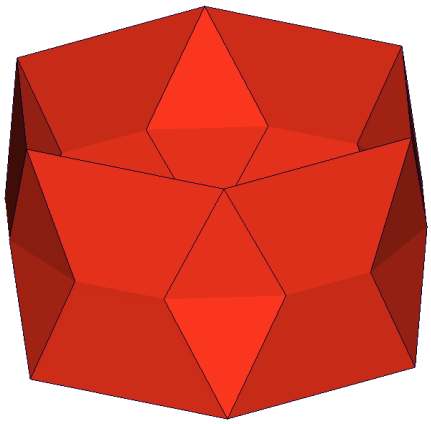

Figure 4 – Origami pattern for hexagonal (N=6) tubes

Ma (2011) investigation defined some variations of the basic pattern presented on Fig. 3. One of these variations is the 6-sided module in Fig. 4. The author performed a parametrical analysis on 5 different standard-groups: square tubes (30 variations), rectangular tubes (4 variations), n-sided polygonal tubes (3 variations) and two types of tapered tubes (8 variations). Moreover, the author analyzed the influence of c/l, l/b and b/t ratio, the angle 2θ, the cross-section and shape of the tubes, external factors over the crushing patterns and the mean force for each tube.

It is proposed here to design an optimized energy absorber tube with a geometry based on the origami pattern proposed by Ma (2011), through techniques of Design of Experiments (DOE) and surrogate models (metamodeling). The optimization is developed according RCAR low-speed structural crash test protocol. A barrier of 1400 kg is driven towards the crash management system, at a 10 degrees' angle, at a speed of 15 km/h. The car model is a simplified rigid body, fixed to a concentrated mass at a distance equal to the center of gravity of a real car, with mass and inertia properties of said car (Fig. 6). The system consists of two Origami Crash Boxes, connected to the car model and to an adapted crossbeam – see Fig. 7.

Metamodel

When a numerical simulation is repeated until a set of design parameters that provide the best virtual performance is found, then an optimization was performed. The flowchart for an optimization process is defined by Cavazzuti (2013) according to the Fig. 5.

The basic configurations for the optimization loop, which was coordinated by modeFRONTIER, are:

Identify the problem: Maximize the energy absorbed by the crash box, while minimizing the peak force.

Define the input parameters: Parametrized geometry of the tubes, according to the variations of the origami basic pattern defined in Fig. 3; boundary conditions and initial load. Most input parameters are defined in the RCAR low-speed structural crash test protocol

Define the input variables: All of the input parameters can be taken as input variables. However, as Cavazzuti (2013)

remarks, it must be kept in mind that the complexity of an optimization problem grows exponentially with the number of variables. Thus, the number of input variables should be kept as low as possible and a preliminary study to asses which are the most important ones could be valuable. In this case, the set of the input variables can be a subset of the input parameters.

Build the simulation environment: The simulation environment consists of:

- Pre-processor: The finite element parametrized model was built in BetaCAE Ansa 18.1.0.
- Solver: The solver used for all the simulations was Virtual Pam-Safe (PAMCrash) 2014.05.
- Post-processor: The simulations were post-processed in Animator 4 2.1.3.
- Optimization software: The simulation was guided using Esteco modeFRONTIER 2016 – the FAST algorithm, to be explained in the next sections.

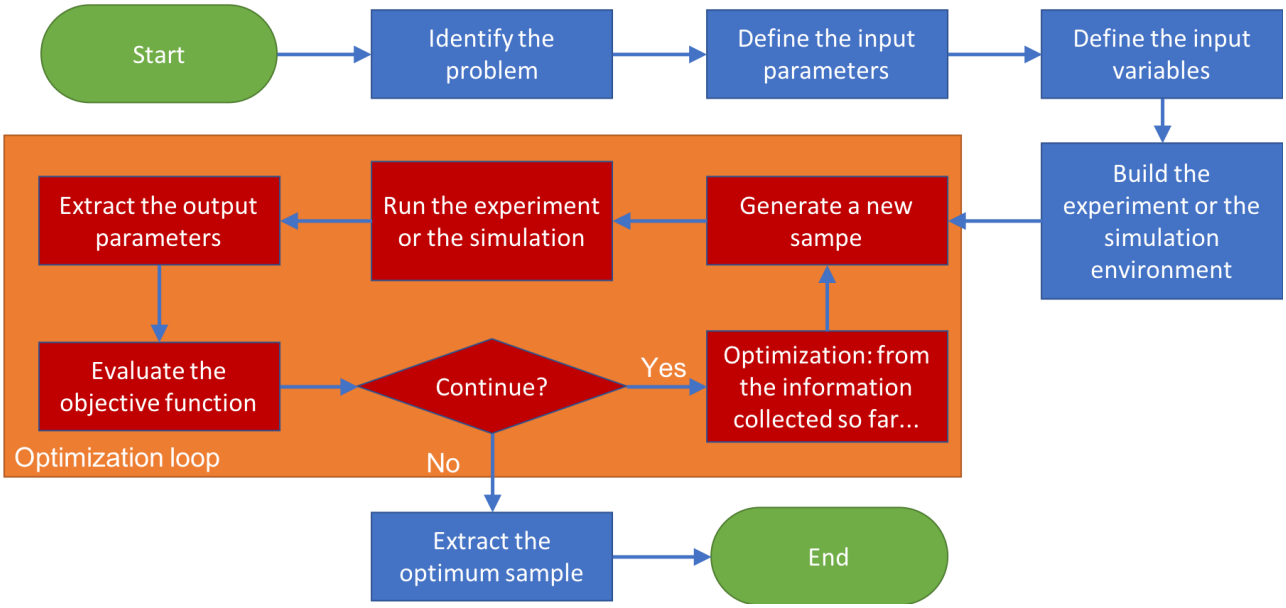

Figure 5 – Optimization flowchart extracted from (Cavazzuti, 2013)

RCAR test model

Ma (2011) evaluated the performance of the tubes with simulations based on an axial impact test, checking the amount of absorbed energy and the average crushing force. In this work, the simulation will be based on the RCAR standard low-speed rear test (RCAR, 2018). The model can be seen in Fig. 6. It includes a whole Crash Management System (CMS), with two crashboxes, one bumper crossbeam, and two plates which connect the CMS to the rest of the body of the car. The car itself was simplified with mass and inertia properties of a compact vehicle (1000 kg, 1504 x 1645 x 3689 mm) attached to a node positioned in the center of gravity of the same vehicle and connected to the plates by a rigid element. The connection elements are represented by the PAMCRASH TIED connectors. The CMS helps reducing the instability during the impact test, due to the connection between the crashboxes, while the simplified car geometry reduces the simulation cost.

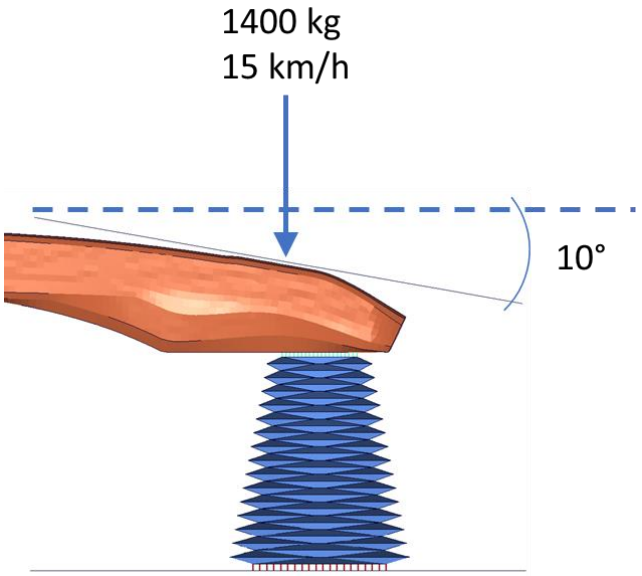

Figure 6– Simulation model – Test conditions

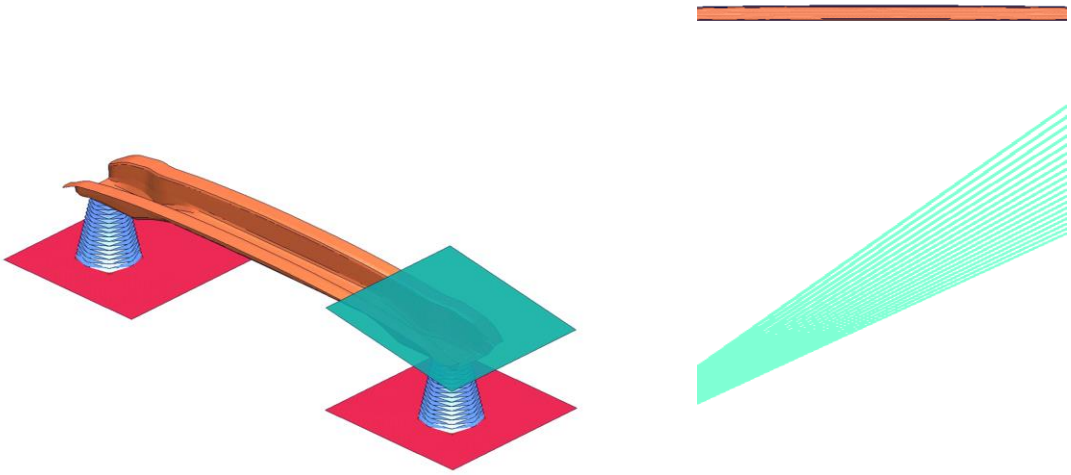

Figure 7– Simulation model – CMS and impactor (left) and rigid body connecting to CG of car (right)

Input Variables

The input variables for the optimization of the origami crashbox are (see Fig. 3):

- l: height of the unit module, before folding;
- b: length of each side of the unit module;
- c: length of the crest;
- t: thickness of the tube;
- N: number of sides of the tube;
- $Taper$: type of tapering;
- $Taper\ Factor$: used to variate the angle of the tapering.

The angle 2θ depends on the relation between these variables. It can be calculated by the following equation:

$$\cos\theta = \tan\left(\frac{\pi}{2N}\right)\frac{c}{l} \tag{1}$$

Numerical simulation of the problem

The simulation conditions were built inside the optimization software modeFRONTIER. The basic workflow is composed by the Process Flow and by the Data Flow. The Process Flow determines the chronological sequence of the

simulations used in the design evaluation process. The Data Flow describes which data should be considered in each step of the Process Flow. The optimization loop is executed every time a design evaluation is required (Esteco, 2016).

As explained in the previous session, the simulation model is a simplified vehicle, with a CMS made of two origami crashboxes and one crossbeam (Fig. 7). The material of the crashbox is considered elastoplastic with isotropic damage (type 105 in PAMCRASH library materials). The model is for shell elements. The required material characteristics were obtained from the experimental properties of material DP-780, a dual-phase automotive steel, as in Table 1. Table 1 shows elastic properties E (Young Modulus), ρ (density), ν (Poisson) and A_s (transverse shear correction factor). Table 2 shows the elastoplastic parameters defined by Calle, Oshiro and Alves (2017), according to the yield stress described by Alves (2000) and defined below,

$$\sigma = \left[k + R_0\varepsilon_p + R_\infty(1 - e^{-b\varepsilon_p})\right]\left[1 + \left(\frac{\dot{\varepsilon}}{D}\right)^{1/p}\right] \quad (2)$$

where k is the initial yield stress; R_0, R_∞ and b are the variables of the (Voce, 1955) material model, ε_p is the equivalent plastic strain, $\dot{\varepsilon}$ is the strain rate and D and p are parameters of the Cowper-Symonds model. Figure 8 show the stress-strain curves with strain rate dependence.

Table 1 – Steel properties

E(GPa)	$\rho\ (kg/mm^3)$	ν	A_s
210	7.85e-06	0.3	0.8333

Table 2 – Adjusted parameters from material law in (Calle; Oshiro; Alves, 2017)

$k\ (MPa)$	$R_0\ (MPa)$	$R_\infty\ (MPa)$	b	$D\ (s^{-1})$	q
492.63	360	550.44	15	19.13	6.21

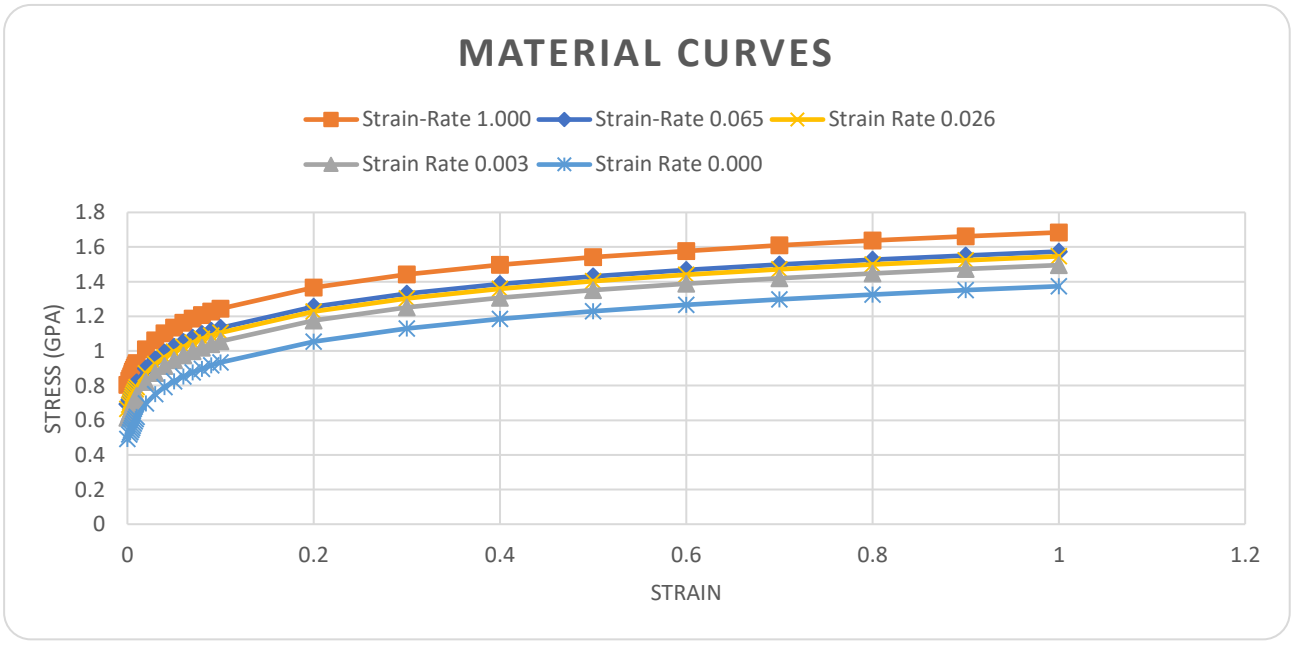

Figure 8 – Material law adjusted for DP780 – strain curves obtained using modified Cowper-Symonds proposed in (Alves, 2000)

Regarding the mesh specifications, information can be checked on Table 3.

Table 3 – Mesh properties

Average of Shells/Model of Crashbox	Average of Nodes/Model of Crashbox	Target Element length	Acceptable Min. Element Length	Acceptable Max. Element Length
4900	4820	5.0 mm	3.5 mm	7.0 mm

Optimization: Objectives

According to Ma (2011), despite the large amount of research done to develop efficient energy absorbers, it remains a challenge to design a system with low initial buckling force, high SEA, stable failure mode, that fits well with the main structure, and can be manufactured at a reasonable cost (see also Lu & Yu (2003)). Focusing on this challenge, the authors defined the objective functions optimization as:

$$maximize\ SEA = \frac{\left(E_{cb}^{def}\right)_{max}}{m_{cb}} \tag{3}$$

$$maximize\ LU = \frac{F_{mean}}{F_{max}} \tag{4}$$

Where F_{max} is the peak force between impactor and CMS during the simulation; δ_{crush} is the maximum crushing distance; E_{cb}^{def} is the internal energy of the crash boxes, absorbed during the impact; m_{cb} is the mass of the crash boxes; F_{mean} is the mean crushing force during the impact, defined as:

$$F_{mean} = \frac{\int_0^{\delta_{crush}} F(x)\,dx}{\delta_{crush}} \tag{5}$$

One will notice that the load uniformity *LU* described here is the inverse of the load uniformity defined in Ma (2011). In this article, the load uniformity was kept in the domain of [0, 1], to avoid numerical issues during the optimization.

Optimization: Constraints

As expected, not all combinations or absolute values are possible. Therefore, a necessary step is to define the domains for each variable, which are:

- $140\ mm \leq Crashbox\ Length \leq 200\ mm$ – limit the length of the Crash Box, based on usual crashbox sizes for common vehicles.
- $40\ mm \leq \frac{b}{\sin\left(\frac{\pi}{N}\right)} \leq 140\ mm$ – limit the radius of the external circumference around the vertices of the crashbox.
- $40\ mm \leq b \leq 100\ mm$ – limit the side size.
- $20\ mm \leq l \leq 180\ mm$ – limit the height of unit module.
- $10\% * b \leq c \leq 90\% * b$ – avoid too small or too big crests.
- $1.5\ mm \leq t \leq\ 2.1\ mm$ – usual tube thickness values for crashboxes.
- $3 \leq N \leq 13$ – limiting the number of sides. Ma (2011) states that when the polygonal tube has more than 12 sides, it behaves like a cylindrical tube.
- $30\% \leq factor \leq 100\%$ – tapering factor.
- $0 < 2\theta < 180^{o}$ – geometric constraint to allow for feasible designs.
- $Modules \leq 20\ units$ – 20 units of a crashbox sized 140 mm would mean a 7 mm height for each unit module.

There is an important point to be considered when variating the number of modules. The module height l and the number of modules are not totally independent variables. The following expression was used to randomly select a quantity of modules, based on the allowed module quantity:

$$h = l \sin\left[\operatorname{acos}\left(\tan\left(\frac{\pi}{2N}\right)\frac{c}{l}\right)\right]$$

$$NumberModules_{max} = floor\left(\frac{200}{h}\right) \tag{6}$$

$$NumberModules_{min} = ceil\left(\frac{140}{h}\right)$$

$$Modules = round[rand() \cdot (NumberModules_{max} - NumberModules_{min}) + NumberModules_{min}]$$

where *h* is the height of the module after folding, *rand()* is a JavaScript function that selects a pseudo-random number between 0 (inclusive) and 1 (exclusive), *floor* is a JavaScript function that rounds down the input argument, *ceil* rounds up the input argument and *round* is a function that rounds a number to the nearest integer.

Optimization loop: Pre-processor

The software BETACAE Ansa 18.1.0 is used to implement commands in python and run a batch file. The algorithm created for this is pictured in Fig. 9. The program reads the new variables, generate mesh and tube geometry and connect to the other parts of the model.

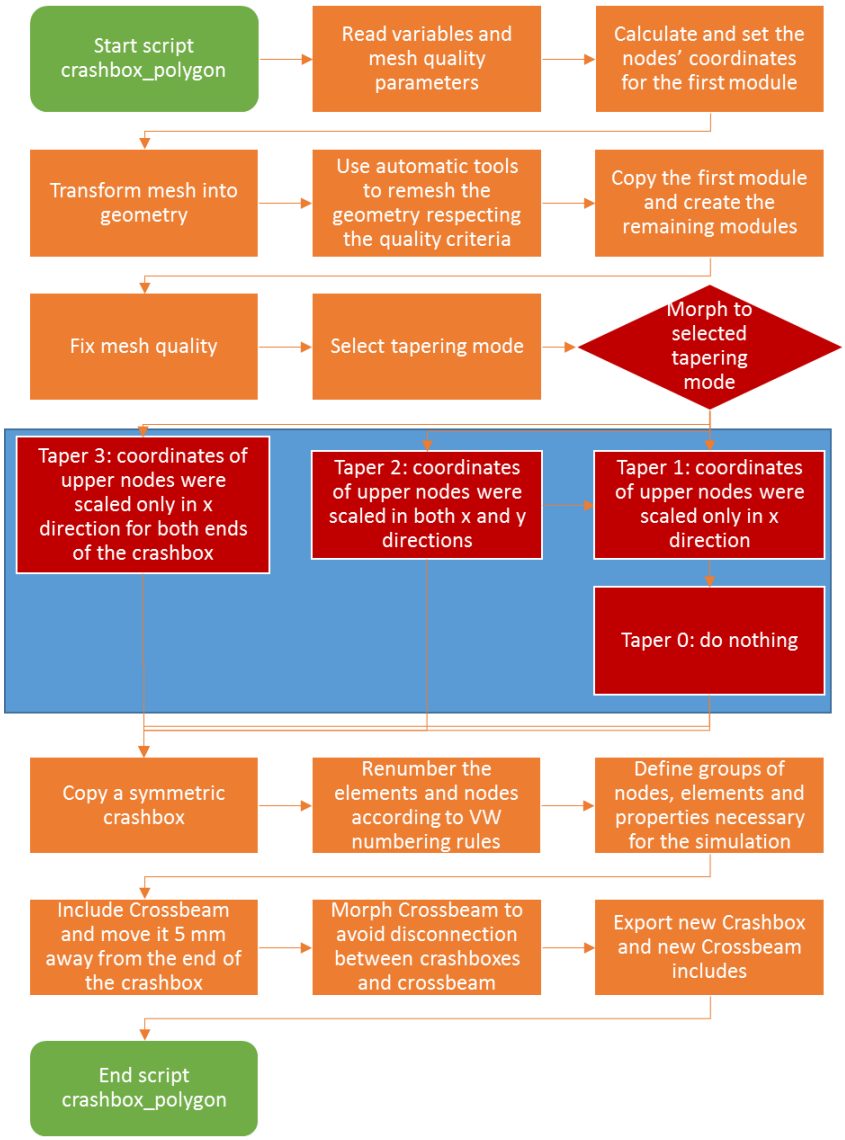

Figure 9 – Ansa Script Workflow for updating the crashbox

Optimization loop: Post-processor

The post-processor software Animator 4 2.1.3 is used to get the following output data,

- Contact force between the impactor and the CMS over time;
- Displacement of the impactor over time;
- Crashbox mass;
- Crashbox Internal Energy over time.

From this information, both the SEA (Eq. 4) and the LU (Eq. 6) could be calculated:

- F_{max} – from contact force
- $F(x)$, δ_{crush}, F_{mean} – from the displacement of the impactor and contact force
- E_{cb}^{def} – from crashbox internal energy

Metamodels – modeFRONTIER FAST algorithm

Montrone, Turco and Rigoni (2014) stated that Response Surface Models (RSM) or Metamodels approach finds a satisfactory set of optimal solutions within a reduced number of evaluations, speeding up the optimization process. A dataset, or training set is used to fit the model, i.e., to learn the system's parameters. Besides, a validation set is necessary to evaluate if the model can correctly solve relevant new examples.

The FAST algorithm available in modeFRONTIER uses the Metamodel approach. FAST main loop is pictured in Fig. 10.

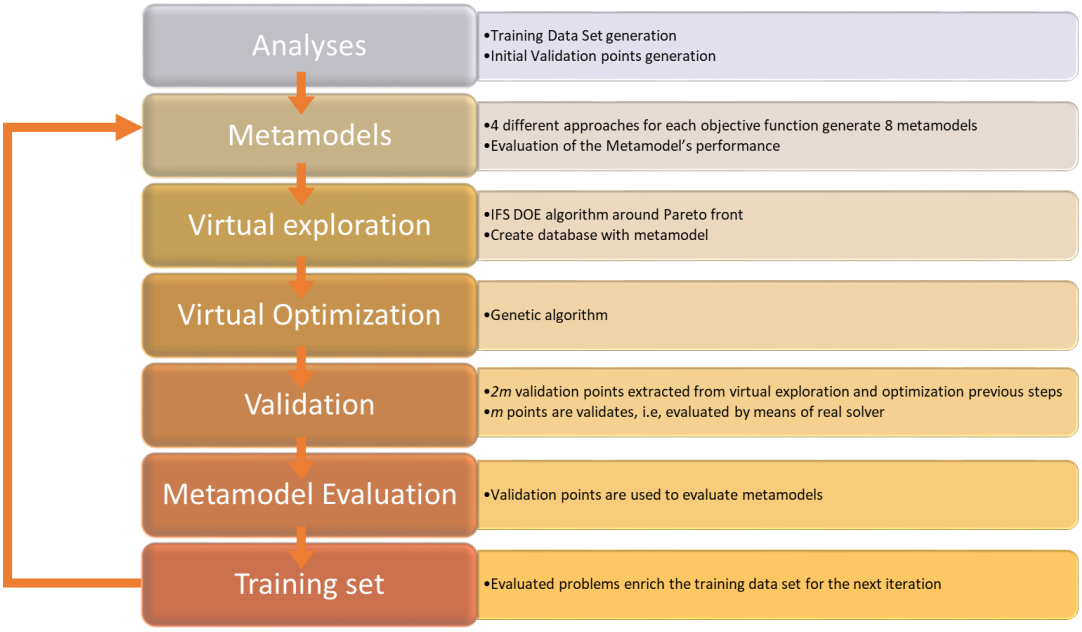

Figure 10 – FAST Algorithm main optimization loop (Montrone; Turco; Rigoni, 2014)

Initially, a training and initial data set are generated, whose input data is based on DOE and output is obtained from numerical simulations of the problem in the PAMCRASH software. Then, four Response Surface Models (RSM) or Metamodels for each objective function are trained with the existing database, using the following methods: Polynomial SVD, Radial Basis Function, Kriging and Neural Networks. A full description of these algorithms is available in (Montrone; Turco; Rigoni, 2014). The performance of the Metamodels is computed by means of the root mean normalized error in the validation points and the best Metamodels are selected for future steps. After that, an Incremental Space Filling algorithm is employed to enrich the space exploration around the Pareto front points. The best *m* points in terms of Pareto ranking and crowding distances are selected for validation process. The next step is to run the called virtual optimization algorithm, i.e., in the algorithm the selected Metamodels are used to approximate the system response. During the Virtual optimization step, a DOE set of size *m*, built up by randomly taking 50% of the current Pareto front points and 50% generated by Random DOE, is used as the initial population of the optimization. Again, the best *m* points in terms of Pareto ranking and crowding distances from the full database evaluated during the virtual optimization are selected for validation process (Montrone; Turco; Rigoni, 2014). During validation process, *m* points, from *2m* previously defined, are randomly selected and validated by means of finite element numerical analyses. The Metamodel performance is evaluated and these *m* points are also used to enrich the training database to be used to the next iteration.

Results

The trade-offs generated by the multi objective optimization result that improving one feature compromises another. The challenge lies in determining the so called Pareto optimal point, i.e., any further improvement cannot be achieved in any of the objectives without degrading at least one of the others (Esteco, 2016). The set of all Pareto points is referred to as the Pareto optimal set and constitute the Pareto frontier in a graphic, as the one showed in Fig. 12. It presents the scatter matrix of the optimization process, with Pareto optimal points highlighted in green. Moreover, the scatter matrix of Fig. 11, as stated in (Esteco, 2016), is a very useful tool for verifying whether there is any linear relation among variables. The Scatter matrix is plotted together with the regression line and helps one to visualize the optimal solutions and understand how they are distributed in the space.

Most influential factors – scatter matrix

According to Fig. 11, one can conclude that the *l* variable strongly correlates with the quantity of Modules. Since the number of modules is limited by the length of the crashbox, this is expected.

SEA is strongly correlated with the number of sides, N. Since SEA is calculated by the rate between the absorbed energy and the crashbox mass, and the crashbox mass (defo mass) has a positive correlation with the number of sides, the negative correlation between SEA and N, b, t and the quantity of modules is expected – see Fig. 11.

The positive correlation between the crashbox mass and the load uniformity LU is also expected. The heavier the crashbox, the more likely it is to have a smaller difference between the peak force and the mean crushing force.

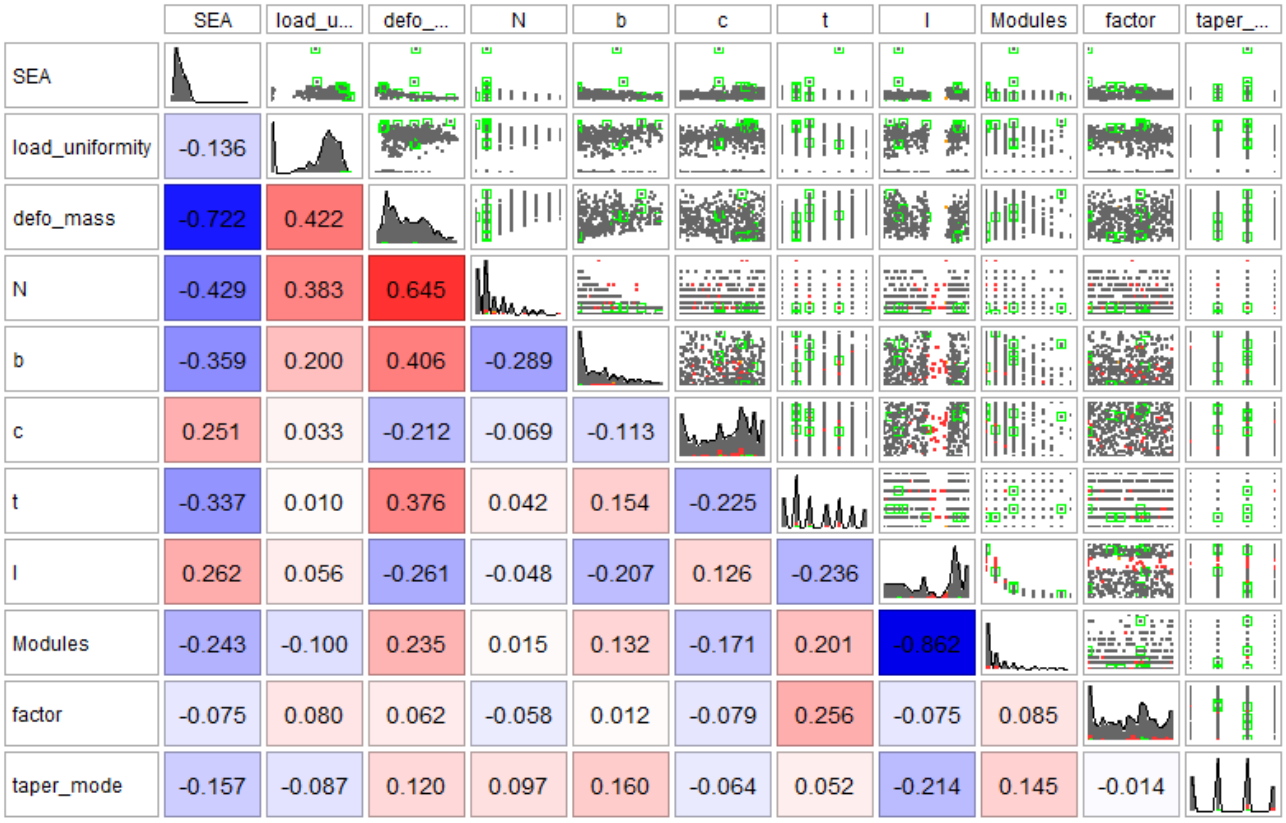

Figure 11 – Scatter matrix of input and output variables

Outliers – SEA, Load Uniformity and unfeasible models

Figure 12 shows LU versus SEA for the optimized final configurations. Even though the optimization software removed several unfeasible designs during the optimization process, there are still some outliers to be noticed here. A near zero value to LU means either the mean crushing force was extremely low during the impact, or the peak force was too high. These situations occur when the crashbox collapses sideways, instead of buckling uniformly, or when the crashbox is too rigid and no plastic deformation is observed. There are also simulations that resulted in a non-realistic SEA. There are two possible limits for the SEA, based on the kinetic energy input of the system and the combination of geometric inputs that result in a possible mass range. These limits are presented on Table 4.

Table 4 – SEA limits

Limit	Initial Kinetic energy (J)	N	t (mm)	b (mm)	Height (mm)	Density (kg/mm^3)	Crashboxes Mass (kg)	SEA (J/kg)
Maximum SEA	12152.8	10	2.1	43.26	140	7.85e-6	0.39564	30717
Minimum SEA	12152.8	3	1.5	40	200	7.85e-6	2.85272	4260

The design configurations resulting in values of SEA out of the limits presented on Table 4 are discarded. They are either disrespecting the crashbox length constraint or the crashbox radius constraint.

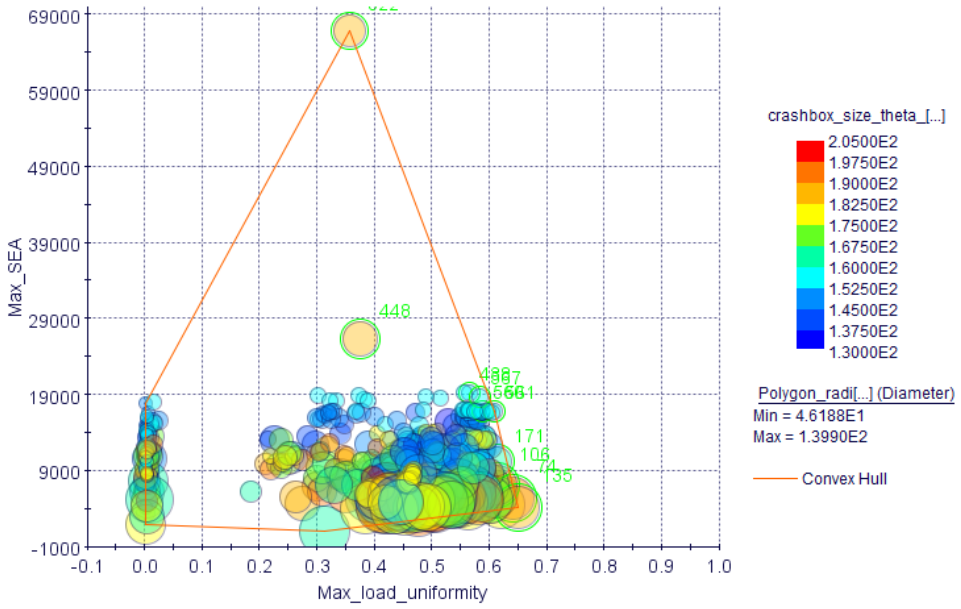

Figure 12 – 4D bubble chart. The color scale refers to the total crashbox length, and the diameter of each circle refers to the radius of the basic polygon of the crashbox.

Pareto frontier

Figure 13 illustrates the Pareto frontier, where the set of optimized parameters are listed in Table 5.

Table 5 – Pareto Front parameters

Id	t (mm)	Modules	N	b (mm)	c (mm)	l (mm)	factor	Taper mode	Polygon diameter (mm)	Crashbox size (mm)
74	1.70	4	4	84.90	62.83	55.60	0.73	2	120.07	196.54
106	1.60	2	3	97.60	46.85	98.60	0.77	1	112.70	189.64
171	1.60	1	4	60.80	48.64	163.50	0.77	1	85.98	162.25
438	1.60	1	4	40.00	26.80	159.60	0.57	2	56.57	159.21
560	1.60	1	4	40.00	30.80	159.30	0.73	1	56.57	158.79
561	1.60	1	4	40.00	30.80	159.30	0.74	1	56.57	158.79
567	1.60	1	4	40.00	28.40	159.60	0.49	2	56.57	159.17

A closer look to Table 5 will show that most of the Pareto Optimal crashboxes have 4 sides, and all of them are tapered, most of them with a tapering factor approximately 75%. However, there's a wide range of both parameters crashbox length and polygon ratio. It leads to a very flexible final design. The designer will be able to analyze other requirements that may not have been taken into account in this optimization. In this work, the best final set of parameters will be chosen analyzing the SEA and LU values.

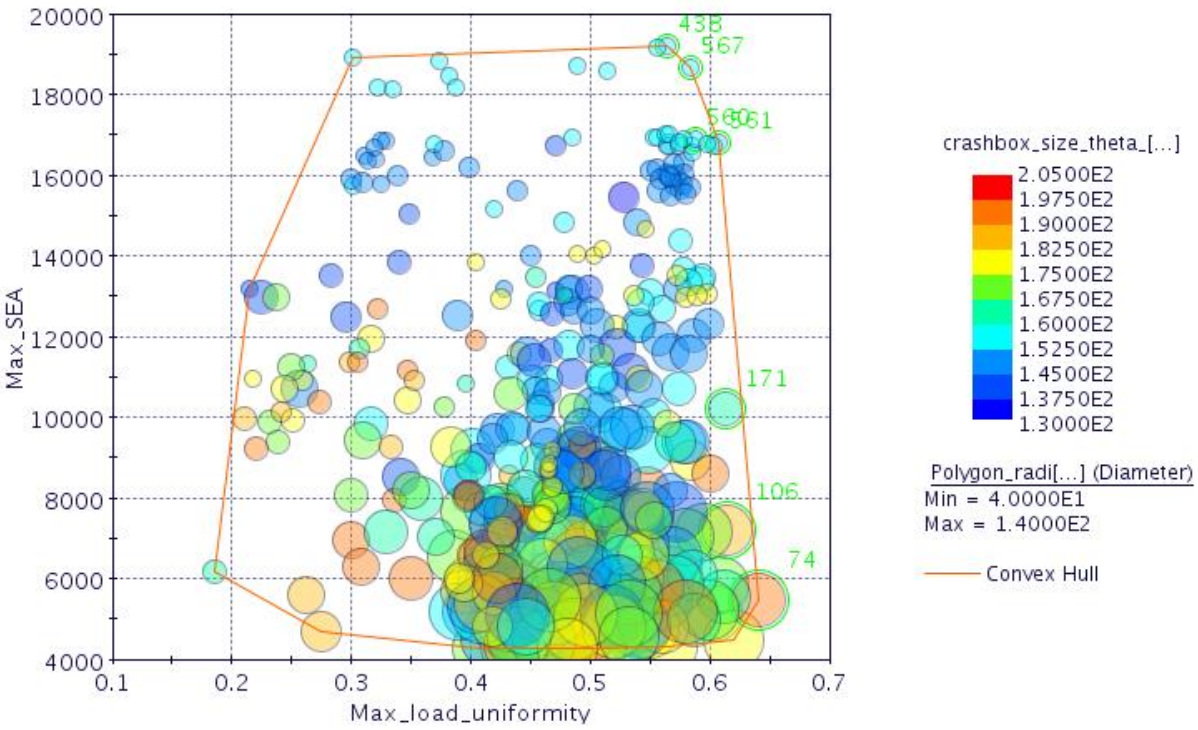

Figure 13 – 4D bubble chart, excluding the outliers. Pareto frontier is highlighted in green.

Final Decision

The output optimal variables for Pareto set are presented in Table 6. All the Pareto front candidates can be seen in Fig. 14. The following criteria can be discussed to decide which is the most convenient Pareto Front set,

- Largest SEA – parameter set #438. It presents the lowest LU from the Pareto front, 0.56. If one is willing to sacrifice a part of SEA, the next candidate with biggest SEA is #567.
- Biggest Load Uniformity – The chosen design would then be #74. It is also the design that presents the lowest SEA amongst the Pareto Set. If one is willing to sacrifice a part of LU, there are three good candidates with an LU of 0.61, and the biggest SEA amongst these candidates is 16841.88 J/kg, candidate #561.
- Smallest crashbox (defo) mass – a common design criteria in industry, the smallest mass amongst the Pareto front candidates is 0.542 kg, from candidate #438.

Two criteria pointed towards the same design, #438. As mentioned in Table 5, this crashbox has thickness of 1.60 mm, 1 module, 4 sides (N), 40.00 mm of each side (b), 26.80 mm of crests (c), 159.60 mm of height before folding (l), tapering number 2 (acting only in one direction on the top of the crashbox), with factor of 0.57. After folding, the overall size of the crashbox was 159.21 mm.

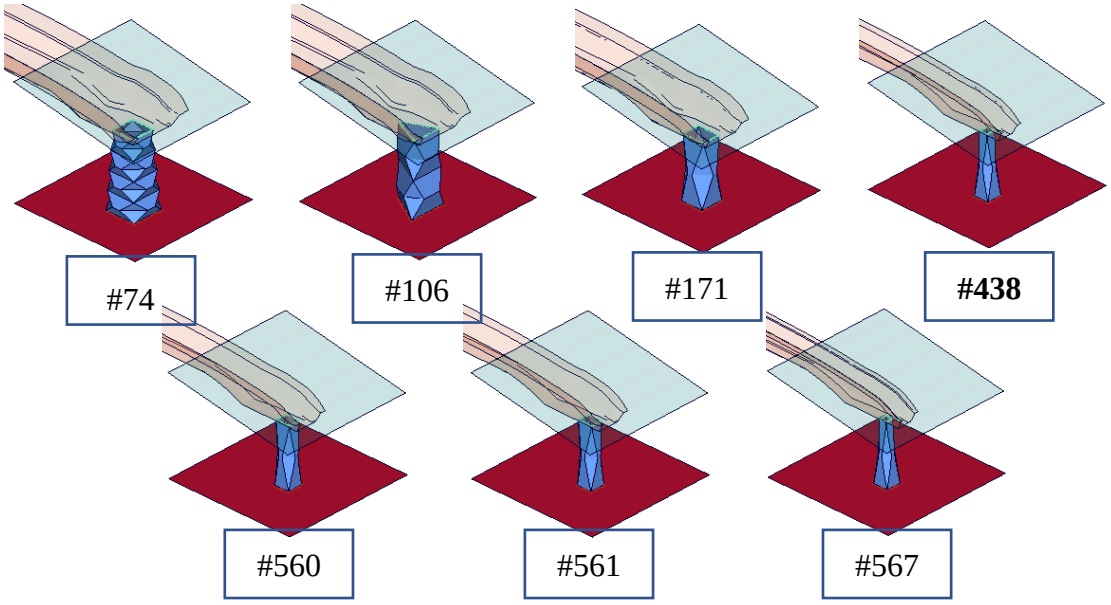

Figure 14 – Pareto Front Origami Crashboxes.

Table 6 – Pareto Front Outputs

Id	Category	Pk (kN)	Pm (kN)	LU	Max energy (J)	Defo mass (kg)	SEA (J/kg)
74	REAL_I1	106.34	68.12	0.64	9362.52	1.713	5465.57
106	VEXP_I1	119.23	73.15	0.61	9837.79	1.365	7207.17
171	VOPT_I2	126.26	77.26	0.61	9650.81	0.944	10226.57
438	VOPT_I6	115.36	65.05	0.56	10416.90	0.542	19215.83
560	VOPT_I8	116.61	68.54	0.59	10192.80	0.603	16895.08
561	VOPT_I8	116.45	70.71	0.61	10182.60	0.605	16841.88
567	VOPT_I8	111.44	64.98	0.58	10504.30	0.562	18690.93

Comparison to a crashbox from industry

A crashbox with the geometry inspired on a real car part was modeled and submitted to the same initial conditions and material parameters. The overall dimensions are listed in Table 7. Figures 15 and 16 show, respectively, the optimized and real crashbox before and after impact.

Table 7 – Crashbox from Industry parameters

Id	t (mm)	Modules	N	b (mm)	c (mm)	l (mm)	factor	Taper mode	Polygon diameter (mm)	Crashbox size (mm)
-	1.70	1	4	100.6	8.49	183.8	0.67	2	113.9	196.54
438	1.60	1	4	40.00	26.80	159.60	0.57	2	56.57	159.21

Table 8 – Pareto Front Outputs

Id	Category	Pk (kN)	Pm (kN)	LU	Max energy (J)	Defo mass (kg)	SEA (J/kg)
-	INDUSTRY	159.1	92.75	0.58	10213.30	2.170	4707.674
438	VOPT_I6	115.36	65.05	0.56	10416.90	0.542	19215.83

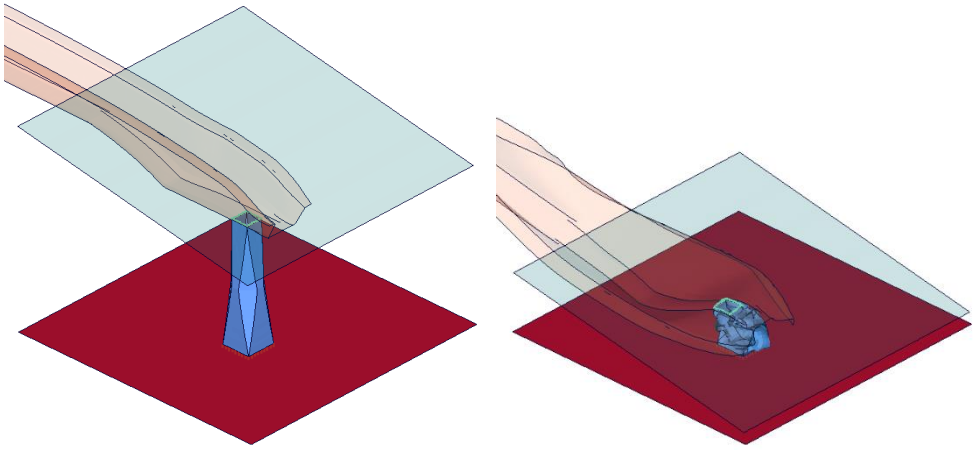

Figure 15 – Design #438 – before crash (left) and at max deformation (right)

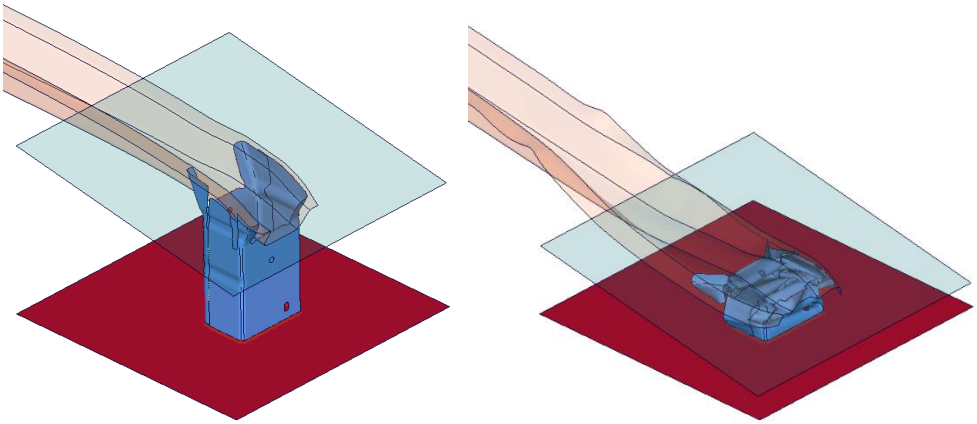

Figure 16 – CMS from industry – before crash (left) and at max deformation (right)

According to the performance parameters in Table 8, the optimal solution proposed here #438 absorbs as much energy as the CMS from industry, with a similar load uniformity and four times less mass.

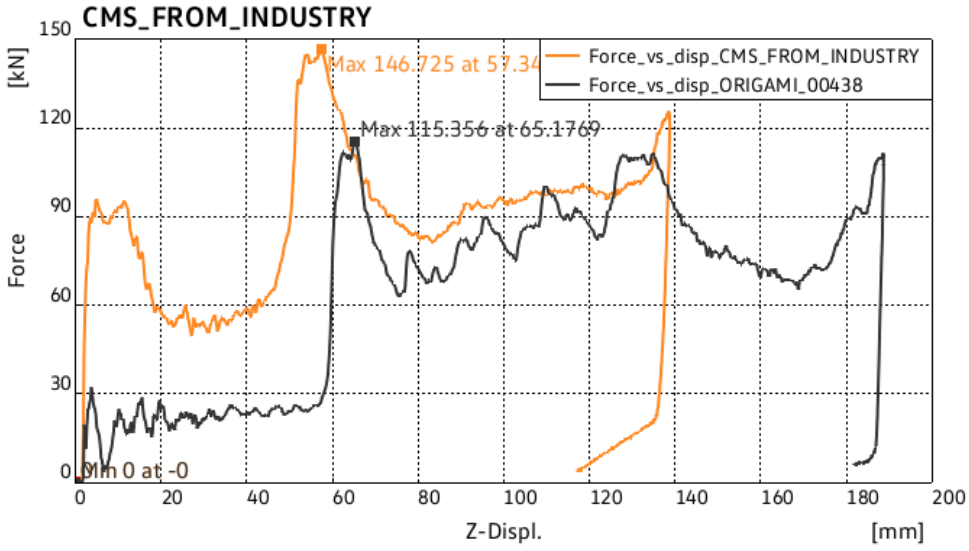

Figure 17 – Comparison between Force vs displacement curves of chosen Pareto design (#438) and CMS from Industry

Figure 17 shows the curves of Impactor Contact Force versus Impactor displacement for both designs. It's easy to notice that the impactor contact force in CMS from industry crash is bigger than the impactor contact force in Origami #438. Also, the total crush length is bigger in Origami #438, which allows a smaller average Force.

CONCLUSION

It is clear from Fig. 13 and Table 6 that the optimization for the origami crashbox has a poor convergence. The Pareto front is formed by designs from several different stages of the optimization process, and different iterations also, as presented in the "category" column. modeFRONTIER names the category as ALGORITHM_STAGE_ITERATION. The Algorithm part was suppressed, since all of the designs in Pareto frontier were generated by the FAST-MOGA2 algorithm. The Stage part can be either real (validated with a solver simulation) or virtual (generated through Metamodels), and in virtual models it can be created during the exploitation or the optimization of the Metamodel. It's rather direct to observe that designs from iteration 1 to 8 were able to make it to the Pareto front.

Nevertheless, even with a poor convergence, the designer is able to have a feeling of the problem, and gather enough information to decide which design is the best solution, based on the decision criteria. The crashbox #438, chosen based on the decision criteria presented on last section (mass, SEA and LU) has four times less mass than the crashbox from industry, therefore presenting a SEA four times bigger than the same crashbox. If another crashbox happened to be selected by different decision criteria, for instance the design #135, manufacturing issues would be a main concern. (Ma, 2011) suggested a hydroforming method for manufacturing the crashboxes.

It's important to notice that other criteria are important when developing a product for industry. The barrier intrusion must be limited so that the parts around the bumper aren't damaged, in order to keep the repair cost low. The crashbox must not present lateral instabilities. Also, it is of utmost importance to perform the simulations with a complete vehicle model, and verify the simulation results with a physical crash test.

ACKNOWLEDGMENTS

We'd like to thank the support of the companies whose software were used in this work.

REFERENCES

ABRAMOWICZ, W.; WIERZBICKI, T. Axial crushing of foam-filled columns. **International Journal of Mechanical Sciences**, v. 30, n. 3, p. 263–271, 1988. Disponível em: <http://www.sciencedirect.com/science/article/pii/0020740388900598>.

ALGHAMDI, A. A. A. Collapsible impact energy absorbers: an overview. **Thin-Walled Structures**, v. 39, n. 2, p. 189–213, 2001. Disponível em: <http://www.sciencedirect.com/science/article/pii/S0263823100000483>.

ALVES, M. Material constitutive law for large strains and strain rates. **Journal of Engineering Mechanics**, v. 126,

n. 2, p. 215–218, 2000.

ASANJARANI, A.; MAHDIAN, A.; DIBAJIAN, S. H. Comparative analysis of energy absorption behavior of tapered and grooved thin-walled tubes with the various geometry of the cross section. **Mechanics of Advanced Materials and Structures**, p. 1–12, 29 jun. 2018. Disponível em: <https://doi.org/10.1080/15376494.2018.1488311>.

BOIS, P. Du; CHOU, C. C.; FILETA, B. B.; KHALIL, T. B.; KING, A. I.; MAHMOOD, H. F.; MERTZ, H. J.; WISMANS, J.; PRASAD, P.; BELWAFA, J. E. Vehicle Crashworthiness and Occupant Protection. 2004.

CALLE, M. A. G.; OSHIRO, R. E.; ALVES, M. Ship collision and grounding: scaled experiments and numerical analysis. **International journal of impact engineering**, v. 103, p. 195–210, 2017.

CAVAZZUTI, M. **Optimization Methods: From Theory to Design Scientific and Technological Aspects in Mechanics**. [s.l.] Springer-Verlag Berlin Heidelberg, 2013.

COMI, C.; DRIEMEIER, L. Wave propagation in cellular locally resonant metamaterials. **Latin American Journal of Solids and Structures**, v. 15, n. 4, 2018.

ESTECO. **ModeFRONTIER 2016 user's manual**, 2016. .

GHANNAM, M. Y.; CLARK, T.; REDDY, Y.; LEE, J. **A Study of Crash Energy and Severity in Frontal Vehicle-To-Vehicle Crash Tests**SAE International , , 2011. . Disponível em: <https://doi.org/10.4271/2011-01-0541>.

HSU, S. S.; JONES, N. Dynamic axial crushing of aluminium alloy 6063 - T6 circular tubes. **Latin American Journal of Solids and Structures**, v. 1, n. 3, p. 277–296, 2004.

ISAAC, C. W.; OLUWOLE, O. Energy absorption improvement of circular tubes with externally press-fitted ring around tube surface subjected under axial and oblique impact loading. **Thin-Walled Structures**, v. 109, p. 352–366, 2016. Disponível em: <http://www.sciencedirect.com/science/article/pii/S0263823116302208>.

KARAGIOZOVA, D.; ALVES, M. Dynamic Elastic-Plastic Buckling of Structural Elements: A Review. **Applied Mechanics Reviews**, v. 61, n. 4, p. 40803–40826, 8 jul. 2008. Disponível em: <http://dx.doi.org/10.1115/1.2939481>.

KOKKULA, S.; LANGSETH, M.; HOPPERSTAD, O. S.; LADEMO, O. G. Behaviour of an automotive bumper beam-longitudinal system at 40% offset impact: An experimental and numerical study. **Latin American Journal of Solids and Structures**, v. 3, n. 1, p. 59–73, 2006.

LANZERATH, H.; SCHILLING, R. **Crash Simulation of Structural Foam**SAE International , , 2003. . Disponível em: <https://doi.org/10.4271/2003-01-0328>.

LEE, S. J.; LEE, H. A.; YI, S. Il; KIM, D. S.; WON YANG, H.; PARK, G. J. Design flow for the crash box in a vehicle to maximize energy absorption. **Proceedings of the Institution of Mechanical Engineers, Part D: Journal of Automobile Engineering**, v. 227, n. 2, p. 179–200, 2013.

LU, G.; YU, T. X. **Energy Absorption of Structures and Materials**. [s.l.] Elsevier, 2003.

MA, J. **Thin-walled Tubes with Pre-folded Origami Patterns as Energy Absorption Devices**. 2011. Doctor of University of Oxford, 2011.

MA, J.; SONG, J.; CHEN, Y. An origami-inspired structure with graded stiffness. **International Journal of Mechanical Sciences**, v. 136, p. 134–142, 1 fev. 2018. Disponível em: <https://www.sciencedirect.com/science/article/pii/S0020740317332599>. Acesso em: 23 out. 2018.

MA, J.; YOU, Z. A Novel Origami Crash Box with Varying Profiles. In: International Design Engineering Technical Conferences and Computers and Information in Engineering Conference, Portland, Oregon, USA. **Anais**... Portland, Oregon, USA: ASME, 2013.

MATSUMOTO, A. T.; DRIEMEIER, L.; ALVES, M. Performance of polymeric reinforcements in vehicle structures submitted to frontal impact. **International Journal of Crashworthiness**, v. 17, n. 5, p. 479–496, 2012.

MONTRONE, T.; TURCO, A.; RIGONI, E. Technical Report 2014-001 FAST Optimizers : General Description. 2014.

RCAR. **RCAR Bumper Test Procedure**RCAR, , 2018. . Disponível em: <http://www.rcar.org/Papers/Procedures/RCAR Bumper Test Procedure Issue 2_1.pdf#zoom=80%25>.

REID, S. R.; REDDY, T. Y.; GRAY, M. D. Static and dynamic axial crushing of foam-filled sheet metal tubes. **International Journal of Mechanical Sciences**, v. 28, n. 5, p. 295–322, 1986.

SADJAD, P.; MOHAMMAD-HOSSEIN, E.; SOBHAN, E.-M. Crashworthiness of double-cell conical tubes with different cross sections subjected to dynamic axial and oblique loads. **Journal of Central South University**, v. 25, n. 3, p. 632–645, 2018.

SHINDE, R. B.; MALI, K. D. An Overview on Impact Behaviour and Energy Absorption of Collapsible Metallic and Non-Metallic Energy Absorbers used in Automotive Applications. In: IOP Conference Series: Materials Science and Engineering, 1, **Anais**...IOP Publishing, 2018.

TARLOCHAN, F.; RAMESH, S. Composite sandwich structures with nested inserts for energy absorption application. **Composite Structures**, v. 94, n. 3, p. 904–916, 2012.

THORTON, P. M.; MAHMOOD, L.-L. F.; MAGEE, C. L. Energy absorption by structural collapse. In: **Structural Crashworthiness**. London: Butterworths, 1983. p. 96–117.

VIGNESH, S.; RAO, C. L.; BADE, S. Energy Absorption Characteristics of AA7075-T6 Tube Filled with Aluminum Foam. In: **Advances in Structural Integrity**. [s.l.] Springer, 2018. p. 303–313.

VOCE, E. A practical strain hardening function. **Metallurgia**, v. 51, p. 219–226, 1955.

WITTEMAN, W. J. **Improved Vehicle Crashworthiness Design by Control of the Energy Absorption for Different Collision Situations**. [s.l: s.n.]

ZHOU, C.; WANG, B.; MA, J.; YOU, Z. Dynamic axial crushing of origami crash boxes. **International Journal of Mechanical Sciences**, v. 118, p. 1–12, 2016.

RESPONSIBILITY NOTICE

The authors are the only ones responsible for the printed material included in this paper.